RILEM
technical letters

Quantitative description of the effect of slag surface area on its reaction kinetics in sodium silicate-activated materials

Abdelrahman Hamdan[1], Taehwan Kim[1]*, Ailar Hajimohammadi[1]

[1] Centre for Infrastructure Engineering and Safety, School of Civil and Environmental Engineering, University of New South Wales, Sydney, NSW 2052, Australia

Abstract

The effects of chemical oxides and the surface area (SA) of slags on the initial reactivity of alkali-activated materials (AAMs) are coupled. It is well known that the reactivity of slag in AAMs is impacted by the SA, however, a quantitative measure of this effect was not provided in previous studies. For a proper understanding of the effect of slag chemistry on the reaction kinetics of AAMs, a quantitative description of the slags SA's effect is required. The reaction kinetics in the activated slags were monitored using isothermal calorimetry. The SAs of the pulverised slags were linked to the time-to-reach-the-main-peak (TTRP) of the reaction, the slope of the acceleration part of the main peak, and the total heat at one, three, and seven days. A 100% relative increase in SA caused a ~51%-75% relative decrease in TTRP. The slope of the acceleration stage also considerably increased with the SA of the slags. However, the effect of the SAs on the total heat was only distinct up to three days and then considerably reduced at seven days. The result of this study indicates that the effect of SA on the initial reactivity of AAMs cannot be simply considered using the proportional contribution. The outcome of this study can provide a promising measure to decouple the effects of SAs and the chemical compositions of slags on the reaction kinetics of AAMs by providing quantitative results for the effect SAs.

Keywords: Surface Area; Alkali-Activated Materials; Reaction Kinetics; Slag; Reactivity

1 Introduction

The cement industry is responsible for nearly 8% of anthropogenic CO_2 [1] due to the decarbonisation of limestone and the energy-intensive process of clinker manufacturing. One of the solutions to curb such high CO_2 emissions is to promote the use of alternative low-CO_2 cements to replace ordinary Portland cement in many applications [2,3]. Alkali-activated materials (AAMs) are proposed as a promising alternative for sustainable cementitious materials production, owing to their lower CO_2 emissions and enhanced mechanical and durability characteristics [4,5]. The activator's chemistry [6–11] and the chemical and mineralogical characteristics of the precursors [12–20] used in AAMs manufacturing are among the most influential factors that control the reactivity and mechanical properties of the resulting binders. Many precursors like granulated blast furnace slag (GBFS) and fly ash were recognised as suitable candidates for AAMs manufacturing [21]. However, such industrial by-products exhibit variable chemical compositions and physical properties, rendering the prediction of their behaviour upon alkali-activation complex. For example, the oxide composition variation of the GBFS, which is often described using the quaternary CaO-MgO-Al_2O_3-SiO_2 system, was estimated to be 30-50% for CaO, 1-18% for MgO, 8-24% for Al_2O_3 and 28-38% for SiO_2 [22]. To

understand the effects of such oxides on the reactivity of AAMs, fundamental studies were carried out using industrial samples [12–14,16–19] as well as simplified synthetic glasses consisting only of the four main oxides [15]. A recent study [23] provided a method to synthesise chemically controlled cementitious materials. In addition to the four main oxides, minor quantities of Fe_2O_3, SO_3, TiO_2, Na_2O, and others may present in industrial slags. Synthetic glasses containing controlled quantities of minor oxides were also prepared to investigate the impact of such oxides on the reactivity of sodium silicate-activated materials [20]. However, despite the precise chemical composition and the similar range of surface area, it was difficult to precisely control the surface areas of glasses after grinding [23].

The physical properties like the surface area and the particle size distribution (PSD) of GBFS affect the reaction kinetics and mechanical properties of the resulting binders upon alkali-activation [24–28]. For example, Gjorv [24] observed that increasing the fineness of slags significantly accelerated the early-age strength of the activated slags, where the one-day strength increased from 4.7 to 22.6 MPa as the Blaine fineness increased from 420 to 640 m^2/kg. Moreover, adiabatic calorimetry results demonstrated that the rate of heat development increased as the fineness increased [24]. The influence of slag and fly ash fineness on the strength

development of sodium hydroxide-activated slags/fly ash blends was investigated by Bijen and Waltje [25]. Slag and fly ash samples were ground by dry and wet (using water) grinding processes. Increasing the Blaine fineness of slag from 500 to 1000 m^2/kg resulted in a considerable increase in strength [25]. In addition, dry grinding showed better strength results than water grinding. However, the strength was not affected by the fineness of the fly ash [25]. Wang et al. [27] observed that at a constant w/s ratio, increasing the fineness of slag caused an increase in the strength of sodium silicate-activated samples up to a specific limit. The optimum fineness range for achieving higher strength was 4000-5000 cm^2/g for the acidic and neutral slags and 4000-5500 cm^2/g for the basic slags [27]. The influence of the slag characteristics on the reaction kinetics and mechanical properties of the sodium carbonate-activated slags was evaluated by Yuan et al. [28]. It was concluded that slag Blaine fineness (436-461 m^2/kg) significantly influenced the reactivity of Na_2CO_3-activated slags. Moreover, the initial precipitation of the $CaCO_3$ increased as slag particles became finer [28].

As previously summarised, the effects of the fineness or the surface area of precursors on the strength developments of slag/fly ash have been considered in past studies. However, the effects of the surface area on the reaction kinetics have not been systematically studied while it is well known that increasing the surface area of a precursor increases its reactivity. Although many fundamental studies have been conducted to investigate the effect of the chemistry of slags in alkali-activated materials, the effect of surface areas on the reaction kinetics has not been properly considered in or decoupled from the measures of reaction kinetics, in particular, the heat release obtained by the isothermal calorimetry measurements. Many researchers simply assume that the difference between surface areas of synthetic glasses is negligible or that the effect of the surface area on the dormant period or TTRP is proportional.

Furthermore, a quantitative description of the influence of the surface areas of slags on the reaction kinetics upon alkali activation has not been previously reported. For example, doubling the surface area of a precursor would not ensure that the dormant period (DP) and the time to reach the main reaction peak (TTRP) are going to proportionally decrease upon alkali activation. Therefore, the quantitative information on the effect of SA on the reaction kinetics is essential, to decouple the effect of the surface area and oxide composition of precursors, which is necessary to properly understand and interpret the influence of a specific oxide on the reaction kinetics of AAMs.

The gas adsorption technique is being increasingly used to determine the precursors' surface areas. However, most research on the role of slag fineness or surface area was carried out by determining the Blaine fineness. Therefore, this study was undertaken to quantify the influence of surface areas of slags on the reaction kinetics in AAMs using Brunauer, Emmett and Teller (BET) surface area. For this purpose, two industrial GBFSs were used in this study and their chemical compositions were measured using X-ray

fluorescence (XRF). The industrial GBFS samples were milled for different times to increase their surface areas. Then, X-ray diffraction (XRD) was employed to detect any changes in the mineralogical/amorphous composition after grinding. Also, total attenuated reflection Fourier transformation infrared (ATR-FTIR) spectroscopy was used to study the impact of the grinding on the glassy phase of slags. The Particle size distributions (PSDs) of the slags were measured using laser diffraction (LD). Moreover, the surface area was determined using nitrogen gas adsorption (NGA). The heat release of the sodium silicate-activated slags was measured using isothermal calorimetry.

2 Materials and methods

The two industrial slags used in this study were claimed to be obtained from the same plant but with different batches. Also, the two slags were milled at the manufacturing plants where the BET surface area of slag1 and slag2 were 0.98 and 1.36 m^2/g, respectively. The PANalytical AXIOS spectrometer was used to measure the chemical oxide compositions of the two types of slag by wavelength-dispersive X-ray fluorescence (WD-XRF). The two slags with similar chemical compositions as shown in Table 1 were ground in a dry condition for different times i.e., 3-, 15-, 30- and 45-minutes using Fritsch Pulverisette 6 Planetary Mono Mill at a speed of 400 rev/minute. Thereby, the samples were given names based on the grinding time. For example, the Slag1_15minG indicates that the slag sample belongs to the first type and was ground for 15 minutes. A constant sample weight of ~ 40 g was milled each time. Four balls (each has a diameter of 30 mm) made of tungsten carbide (density is 14.9 g/cm^3) were used to grind the 40 grams of each raw slag in a 250 ml tungsten carbide bowl. The total mass of the four balls was ~ 843 grams and thus the balls' mass to the slag sample mass was ~ 21. It should be noted that milling for extended times may generate excessive heat. Therefore, milling the samples for 30 and 45 minutes was done in stages (each ~ 15 minutes) where the bowel was allowed to cool down to prevent extreme temperatures rise.

Table 1. The chemical compositions of the two types of GBFSs used in this study. The LOI is the loss of ignition at 1050 °C.

Oxide	Slag1	Slag2
CaO	41.22	41.19
MgO	4.62	5.51
Al_2O_3	13.67	13.18
SiO_2	34.82	35.33
Na_2O	0.23	0.28
SO_3	1.12	1.29
K_2O	0.32	0.32
TiO_2	0.71	0.99
Fe_2O_3	0.61	0.4
LOI	0.59	0.9

The XRD patterns of the raw slags and the samples ground for 30 and 45 minutes were recorded using a PANalytical Empyrean instrument fitted with a copper tube system operated at 45 kV and 40 mA. The XRD patterns were recorded from 10 to 70° 2θ range with a step size of 0.026° and a scan speed of 0.0677 °/second. FTIR spectra of the raw slags were recorded using total attenuated reflection Fourier transformation infrared (ATR-FTIR) spectroscopy by PerkinElmer FT-IR spectrometer fitted with diamond/ZnSe universal ATR accessory. The average of four scans was taken for each spectrum that was recorded between 650 and 4000 cm^{-1} wavenumbers with a resolution of 4 cm^{-1}.

The particle size distribution (PSD) was measured using Malvern Mastersizer2000 from Malvern Instruments based on the laser diffraction (LD) method. Isopropyl alcohol which has a refractive index of 1.39 was used as a dispersant medium for the PSD measurement. The slag refractive index and absorption factor were chosen to be 1.56 and 0.1, respectively. The obscuration level was ~10% and the sonication time and the stirring rate were selected to be 2 minutes and 1700 rpm, respectively. These parameters were chosen based on the recommendation of Arvaniti et al. [29]. The surface areas were determined by the nitrogen gas adsorption method carried out at 77 K (maintained by liquid nitrogen) using the NOVAtouch^{TM}LX^4 gas sorption analyser from Anton Paar. The Brunauer, Emmett and Teller (BET) theory [30] was used to calculate the surface area of each sample based on an 11-point adsorption isotherm for a relative partial pressure range between 0.05 and 0.3. Before measurements, each sample was degassed and heated at 150 °C for ~10 hours to remove gasses and moisture physically adsorbed on the surface of the particles. Two measurements were done per sample, and the average was recorded as the BET surface area.

All samples were then activated using a mixture of sodium hydroxide and sodium silicate. The silica modulus in the activator, i.e., M$_s$ (SiO$_2$/Na$_2$O by weight) was 1.0, and the sodium content defined as Na$_2$O/binder ratio was 0.045. The water-to-solid (w/s) ratio in the mix was 0.40. The TAM Air calorimeter (TA instrument) was used to record the heat flow at 23 °C for 7 days. Quartz which had a specific heat capacity of 0.71 J/(K.g), was chosen to be the reference. The reactants (resulting in a paste of ~ 6.1 g) were mixed by hand inside the ampoule for ~ 2 minutes, shaken using a vortex mixer for another ~ 30 seconds for further homogenisation and then inserted into the TAM channel. The heat flow values were recorded after 45 minutes to avoid the effect of thermal disturbance caused by the insertion of the ampoule inside the TAM channel. The total accumulated heat curves were determined based on heat flow recorded after 45 minutes from the addition of the activator to the slags. Therefore, the recorded heat flow values are expected to be a function of the exothermic reactions between the slags and the activators and no considerable effect of the thermal disturbance on the recorded heat was expected.

3   Results and discussion

The XRD patterns of the unground slags and their corresponding pulverised samples (for 30 and 45 minutes) are shown in Figs. 1 (a) and (b) for types 1 and 2, respectively. All samples are characterised by a scattering diffuse hump centred at 2θ ≈ 31°, indicating the presence of an amorphous content related to the glassy phase presented in the slags. The absence of Bragg reflections indicates that no considerable crystalline phases were presented in the samples.
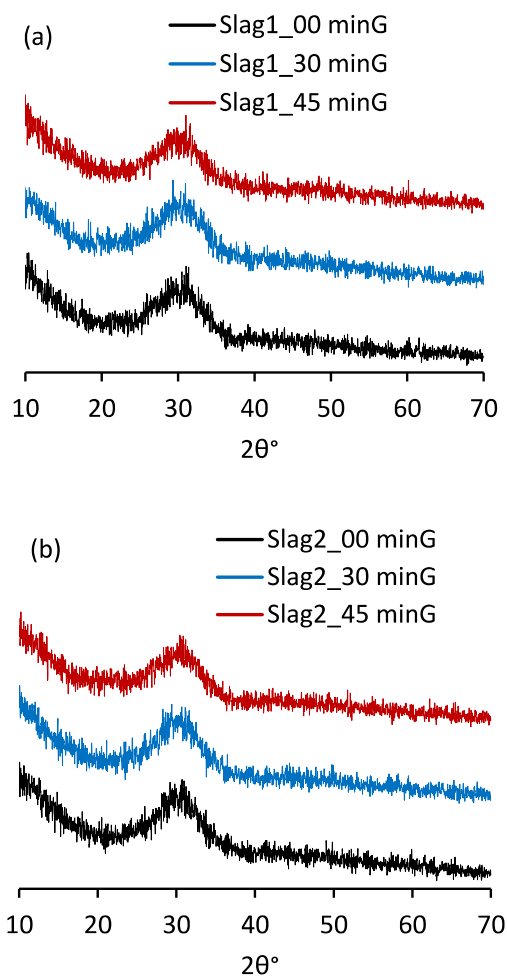
Figure 1. The XRD patterns of type 1 and type 2 slags.

The XRD patterns of the slags ground for 30 and 45 minutes also have the same characteristics where the scattering diffuse maximum was positioned at 2θ ≈ 31° without Bragg reflections. This indicates that grinding has not caused considerable changes to the slag's glassy phase. This was evident as neither a new Bragg reflection was formed nor a shift in the position of the diffuse maxima was observed.

Fig. 2 shows the ATR-FTIR spectra of the slag samples before and after grinding. All samples have a broad spectrum centred at a ~ 910 cm^{-1} wavenumber. The broad resonance is related to silicate species in different polymerisation forms ranging from Q^1 to Q^4 [31]. Since the spectra are centred at ~ 910 cm^{-1}, a considerable part of the silicate specie is present in Q^1 form

[31], [32] where one oxygen atom in the silicon tetrahedra is connected to the silicon or aluminium atom in the neighbouring tetrahedra. As shown in Figs. 1 and 2, no obvious changes or shifts in the XRD and the FTIR spectra of the raw slags are noticed after different grinding times. Therefore, the observed changes in the reactivity among each slag type should be primarily a function of the surface area.

The PSDs of all samples are presented in Fig. 3. Generally, as the grinding time increased, the fineness of GBFS samples increased as expected (especially within the range from 0.1 μm to 10 μm). The D_{10} and D_{50} values for each GBFS also decreased with the grinding time indicating a decrease in the particle size. Above ~ 10 μm size, the agglomeration of small particles of type 1 slag and the air bubbles produced during the sonication may cause experimental errors. Table 2 presents the D_{10}, D_{50}, D_{90}, and LD surface area of the slags. Also, the LD surface area which is calculated based on an equivalent spherical particle shape increased for the two types of slag as the grinding time increased.

The surface areas of the ground samples calculated by BET theory based on the gas adsorption measurements are presented in Table 3. The BET surface areas of unground samples, i.e., Slag1-00minG and Slag2-00minG, were 0.98 and 1.36 m^2/g, respectively. It should be noted that the BET surface area of slags is larger than the LD one as the gas adsorption considers the accessible particle's pore while the laser diffraction method considers only the equivalent spherical shape of the particles.
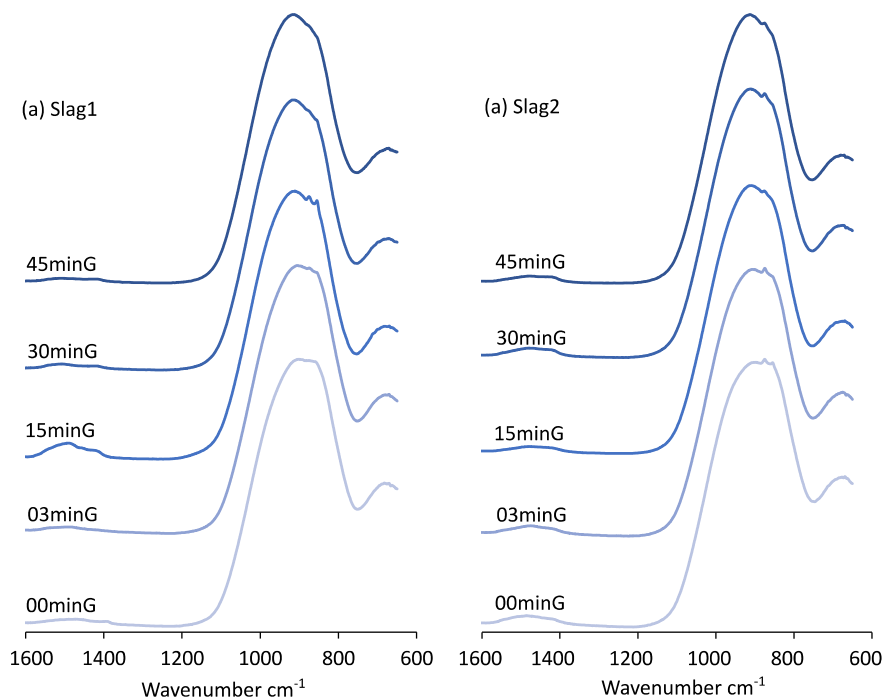
Figure 2. The ATR-FTIR spectra of type 1 and type 2 slags.
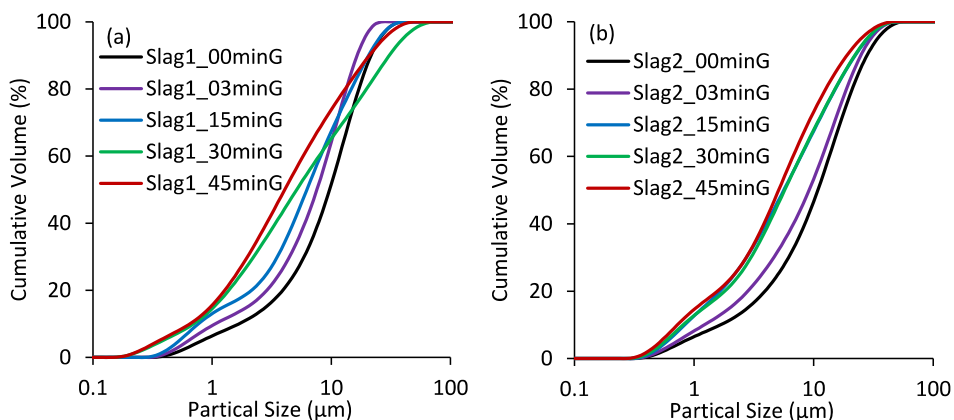
Figure 3. Cumulative particle size distributions by laser diffraction for (a) slag1 and (b) slag2.

Table 2. The D_{10}, D_{50}, D_{90} and LD surface areas of type 1 and type 2 slags.

Sample	D_{10}	D_{50}	D_{90}	LD Surface area (m^2/g)
Slag1_00minG	1.92	11.10	24.75	0.53
Slag1_03minG	1.22	8.70	18.91	0.69
Slag1_15minG	0.88	7.16	23.63	0.85
Slag1_30minG	0.80	5.88	35.63	0.98
Slag1_45minG	0.75	4.67	23.97	1.08
Slag2_00minG	1.91	12.46	32.06	0.51
Slag2_03minG	1.40	10.53	28.45	0.61
Slag2_15minG	0.96	6.47	25.63	0.85
Slag2_30minG	0.93	6.57	25.29	0.85
Slag2_45minG	0.83	5.86	21.82	0.94

Table 3. The BET surface areas of the samples used in this study.

Sample	Surface area (m^2/g)				
	00minG	03minG	15minG	30minG	45minG
Slag1	0.98	1.64	1.84	2.17	2.45
Slag2	1.36	2.00	2.26	2.45	2.62

Each sample's BET surface area was also increased as the grinding time increased, compatible with the increase in the fineness measured by the PSD. After 45 minutes of grinding, the relative increase in the BET surface area of type 1 and type 2 was ~ 150% and ~ 93%, respectively. The differences in the recorded relative surface areas' increase between the two types of slags could probably be the result of the variability of the grinding efficiency and the differences in mechanical characteristics of the slag particles.

The normalised heat flow and the total normalised heat (by the mass of paste) of the activated slags for each type are presented in Fig. 4. The isothermal calorimetry technique is a widely used method to monitor the reaction kinetics of cementitious systems. The occurrence of an initial dissolution peak followed by an obvious dormant period and then, an acceleration/deceleration peak for the liquid sodium silicate-activated slags was demonstrated in many previous studies [12,14,17,33–35]. The calorimetry results shown in Fig. 4 of the current study were comparable to the characteristics of the heat released from the typical sodium silicate-activated slags [12,14,17,33–35].

As shown in Fig. 4 (a) and (c), each heat flow curve is characterised by two peaks. The first peak was caused by the heat of wetting and the fast dissolution of the small slag grains [33]. This pre-induction peak was followed by a dormant period (DP) of variable length depending on the sample i.e., the surface area. This dormant period observed in the sodium silicate-activated slags seems to be the result of the hindrance of the dissolution of Si from the slag due to the abundant soluble Si in the alkaline activator [34]. As the surface area of each slag type increased, the DP was considerably shortened. Afterwards, a second (main) peak was shown, caused by the exothermal reaction due to the precipitation of reaction products. The time to reach the main peak (TTRP) is defined

as the time from the start of the reaction till reaching the maximum heat flow of the second peak.

Although slag1 and slag2 samples had very similar chemical compositions and were composed of an amorphous phase, slag1 consistently reacted faster upon alkali activation despite its lower surface area compared to slag2. The different reactivity of the two slags (despite the comparable oxide composition and amorphous content) could be the result of the different glassy molecular structures. The different thermal history due to variations in the operation parameters such as the molten temperature and different cooling rates of the slags can affect the glassy structures and their reactivity in cementitious systems [36,37]. For example, Ehrenberg et al. [36] found that annealed slags with higher fictive temperatures exhibited an increased reactivity in blended cement compared to annealed slags with lower fictive temperatures. The higher fictive temperature corresponds to fast-cooled samples [36,38]. This indicates that the different cooling rate has a significant effect on the reactivity of slags in cementitious systems [36]. Further research is required to find the fundamental reason for the different reactivity observed for the slags that had practically identical chemical compositions and XRD patterns.

The TTRP and the slope of the acceleration part of the main peak are an indication of the reaction speed. TTRP corresponds to the time taken from the start of the reaction until the onset of the deceleration period. The slope of the reaction curve is related to how fast reaction products i.e., C-(A)-S-H are formed because the acceleration part is related to the formation of the main reaction product. Therefore, the increase in the reaction rate would shorten the TTRP and increase the slope of the acceleration part of the main peak. The total accumulated heat is an indirect indication of the degree of reaction. If the total heat increased, then more

reaction products are assumed to be formed. As the surface of the raw slags increased in the current study, the TTRP decreased, the slope of the acceleration part of the heat release curve increased, and the total accumulated heat increased (as shown in Fig. 4), which indicates a fast reaction and a higher degree of reaction.

Increasing the surface area of the slags considerably changed the reaction kinetics by affecting the DP, the TTRP, and the shape of the second main reaction peak upon alkali-activation. Heat release curves shown in Fig. 4 (a) and (c) demonstrated that TTRP decreased significantly due to the increase in the surface area of slags. However, the decrease in the TTRP was not proportional to the increase in surface area for the two types of activated slags. The activated slags with low surface areas had a broad main peak with low heat flow values. As the surface areas of slags increased, the activated slags exhibited higher heat flow values with narrower heat flow peaks. Moreover, the slope of the acceleration part of the second main peak considerably increased by increasing the surface area. This indicates the fast precipitation of reaction products from the slags of high surface areas. Also, the total accumulated heat increased as fineness increased for the two types of slag, as shown in Fig. 4 (b) and (d).

Fig. 5 (a) shows the relation between the % relative increase in the surface area and the % relative decrease in the TTRP for each sample. A 100% increase in the surface area for slag1 and slag2 caused ~ 51% and ~ 75 % relative decrease in TTRP,

respectively. An increase in the surface area should be related to the relative decrease in the TTRP. This study indicates the relation between the relative increase in surface area and the relative decrease in TTRP could reasonably be described as a linear (but not proportional) relation regardless of GBFS type [red fitted line in Fig. 5 (a)]. The red line represents the % relative decrease in the TTRP for the two activated slag types, i.e., slag1 and slag2. A 100% relative increase in the surface area of slag caused a ~ 58% decrease in the TTRP with R^2 of ~ 0.93.

Despite the limited data in this study, the results indicate that the effect of the surface area on the reaction kinetics can be reasonably decoupled from the effect of the chemical composition using a single linear relationship shown in Fig. 5 (a) regardless of the slag source. However, more data would be required to validate the application of a single linear relationship between TTRP and surface area in activated materials.

The increased reactivity of the slags with the higher surface area was also expressed in terms of the slope of the acceleration part of the heat rate curve as shown in Fig. 5 (b). The fast precipitation of reaction products caused a higher slope of the acceleration stage. As the surface area increased, the acceleration slope exponentially increased, which reflects the influential role of surface areas in speeding up the reaction.
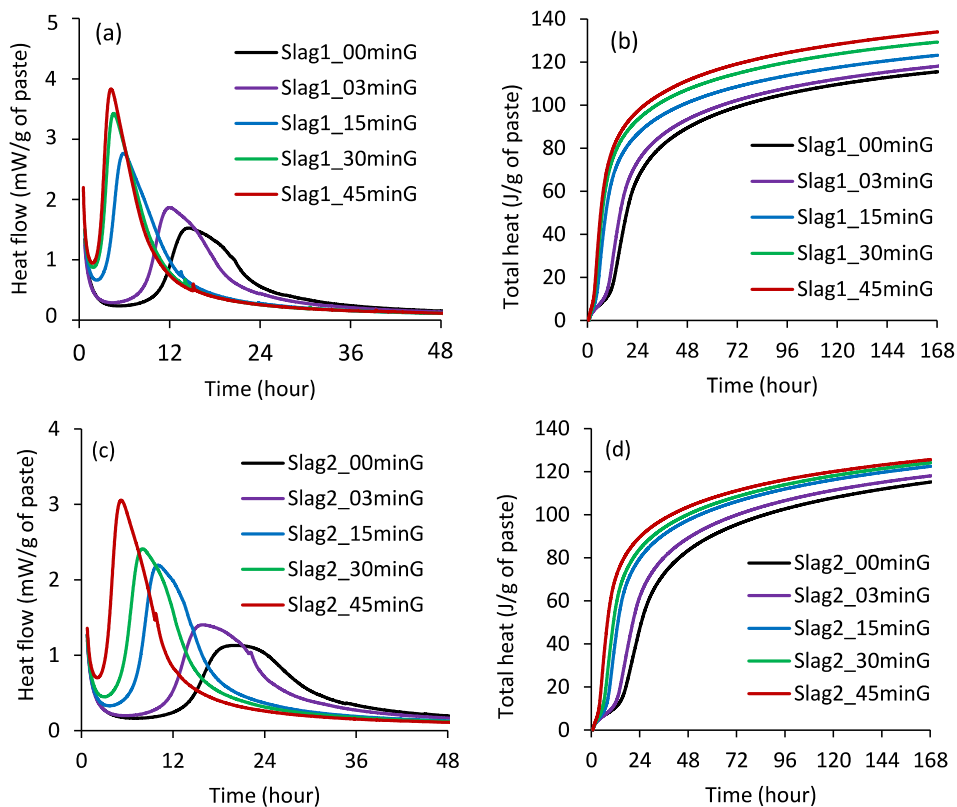
Figure 4. Isothermal calorimetry results of the activated samples: (a) and (c) are heat flow curves of the activated slag1 and slag2 samples, respectively, and (b) and (d) are the total heat of the activated slag1 and slag2 samples, respectively. All results are normalised per gram of paste.
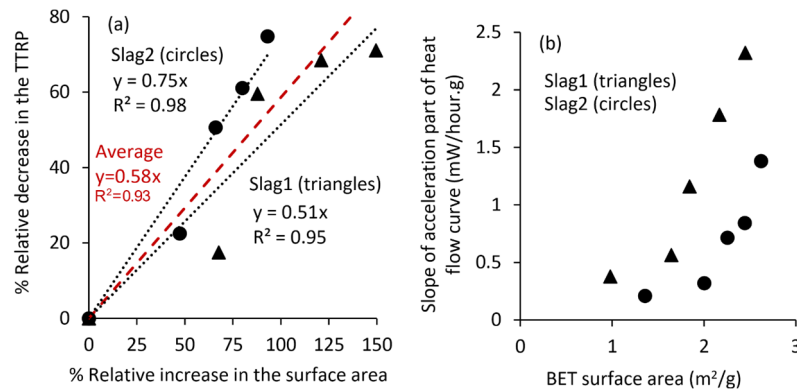
Figure 5. (a) The relative % decrease in the TTRP with the relative % increase in the surface area of each slag type (b) the slope of the acceleration part of the heat flow curve with the BET surface area. Slag1 and slag2 are represented in triangles and circles, respectively.
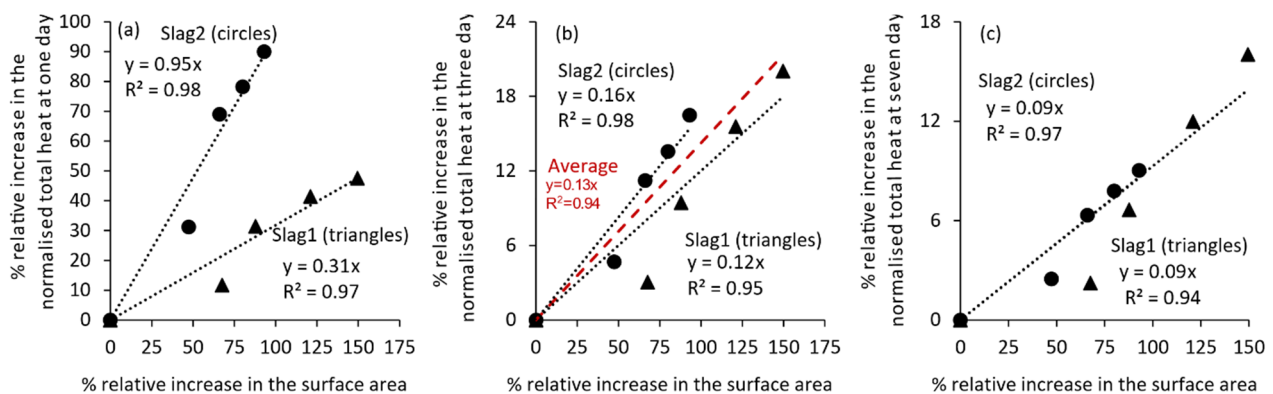
Figure 6. % relative increase in the total heat recorded at (a) one day, (b) three days and (c) seven days with the % relative increase in the surface area of the activated slag1 (triangles) and slag2 (circles) samples.

The change in the surface area caused an increase in the total accumulated heat, as presented in Fig. 6. The test results demonstrated that a 100% increase in the surface area of slag1 caused, on average, a ~ 31%, ~ 12% and ~ 9% increase in the total accumulated heat recorded at one, three and seven days from the start of the reaction, respectively. The corresponding values for slag2 were ~ 95%, ~ 16%, and ~ 9%. Therefore, increasing the surface areas has significantly increased the cumulative heat at a very early age (up to 1-3 days) and their effect on the accumulated heat was significantly reduced at a later age (7 days).

The accumulated heat release can be correlated with the quantity of the reaction products precipitated after the alkali-activation reaction. This in turn is expected to increase the strength of activated samples which was confirmed in past studies [24–28]. Gjorv [24] demonstrated that the increase in the Blaine fineness of slags caused an increase in the temperature recorded for activated slags in adiabatic calorimetry, indicating an increased reactivity. However, Jimenez et al. [39] concluded that the effect of slag's surface area is the least influential factor on strength compared to activator nature, curing temperature or activator concentration. Moreover, the surface area factor was only important for flexural strength and compressive strength up to three days of curing [39]. This agrees well with results shown in Fig. 6 (a), (b) and (c) where the % increase in the total heat decreased from ~ 63% (the average of 95% and 31%) to 9% as the reaction progressed from one day to seven days.

Therefore, the % increase in the total heat due to differences in the surface areas of slags decreased as the reaction progressed. This indicates the effect of surface areas on the accumulated heat (which is usually correlated with the strength of AAM) becomes less important as the reaction progresses, which was consistent with the results of the previous study [39].

4   Conclusion

Although the surface area (SA) of a precursor is known to influence its reactivity in alkali-activated materials, the quantitative effect of the SA was not fully investigated. Furthermore, variations of SAs among different precursors were not given deserved attention in past studies. Such information is critical to precisely investigate the reaction kinetics of the precursors and to compare the reactivities of different precursors in AAMs. This paper fills this gap by providing potential ways to quantitatively decouple the effects of SA when studying the influence of slag chemistry on the reactivity in cementitious systems using calorimetry data. The findings of the current research are novel as it was able to quantitatively link the surface areas of slags to the reactivity of the sodium silicate-activated slags, in particular, the time to reach the second peak (TTRP), the slope of the acceleration part of the heat rate curve, and the total accumulated heat at seven days.

It was found that the 100% relative increase in the SA caused a ~ 51 to ~ 75 % relative decrease in the time to reach the peak

(TTRP). This indicates that the proper decoupling of the effects of chemical oxide composition and the SA should be considered to investigate the effect of the chemical composition on the reactivity of alkali-activated materials. On average, a ~ 58% relative decrease in TTRP due to a 100% relative increase in the SA could be adapted to study the reactivity of alkali-activated slags. The slope of the acceleration stage exponentially increased with the increase in the SA. The surface area of the slags significantly affected the early age reaction kinetics, which may influence the setting time and the very early age strength up to three days. On the other hand, a 100% relative increase in the SA caused only ~ 9% relative increase in the total heat accumulated recorded at seven days, indicating that the effect of the SA on the total accumulated heat at later ages was less significant compared to its effect on the early age reactivity. With the current results of this study, the extent of the SAs' effects on the reactivity of slags in sodium silicate systems could be realised for a better interpretation of the precursor's behaviour in alkali-activated systems. Finally, It was also noted that, although the two slags used in this study had practically identical chemical oxide compositions and similar amorphous contents, slag1 reacted faster than slag2 due to possible differences in the thermal history.

Authorship statement (CRediT)

Abdelrahman Hamdan: Conceptualisation, Methodology, Validation, Formal analysis, Investigation, Data curation, Writing – original draft, Visualization.

Taehwan Kim: Conceptualisation, Methodology, Validation, Formal analysis, Resources, Writing – review & editing, Visualization, Supervision, Project administration, Funding acquisition.

Ailar Hajimohammadi: Conceptualisation, Methodology, Validation, Resources, Writing – review & editing, Supervision, Project administration.

Conflict of interest

The authors declare that they have no conflict of interest.

Acknowledgement

References

[1] J.G.J. Olivier, G. Janssens-Maenhout, J.A.H.W. Peters, Trends in global CO₂ emissions. 2012 Report, 2012. https://doi.org/10.2788/33777
[2] E. Gartner, Industrially interesting approaches to "low-CO₂" cements, Cem. Concr. Res. (2004) 34: 1489-1498. https://doi.org/10.1016/j.cemconres.2004.01.021
[3] K.L. Scrivener, V.M. John, E.M. Gartner, Eco-efficient cements: Potential economically viable solutions for a low-CO2 cement-based materials industry, Cem. Concr. Res. (2018) 114: 2-26. https://doi.org/10.1016/j.cemconres.2018.03.015
[4] J.L. Provis, Alkali-activated materials, Cem. Concr. Res. (2018) 114: 40-48. https://doi.org/10.1016/j.cemconres.2017.02.009
[5] C. Shi, B. Qu, J.L. Provis, Recent progress in low-carbon binders, Cem. Concr. Res. (2019) 122: 227-250. https://doi.org/10.1016/j.cemconres.2019.05.009
[6] M. Ben Haha, G. Le Saout, F. Winnefeld, B. Lothenbach, Influence of activator type on hydration kinetics, hydrate assemblage and microstructural development of alkali activated blast-furnace slags, Cem. Concr. Res. (2011) 41: 301-310. https://doi.org/10.1016/j.cemconres.2010.11.016
[7] A. Fernández-Jiménez, F. Puertas, Setting of alkali-activated slag cement. Influence of activator nature, Adv. Cem. Res. (2001) 13: 115-121. https://doi.org/10.1680/adcr.2001.13.3.115
[8] D. Bondar, C.J. Lynsdale, N.B. Milestone, N. Hassani, A.A. Ramezanianpour, Effect of type, form, and dosage of activators on strength of alkali-activated natural pozzolans, Cem. Concr. Compos. (2011) 33: 251-260. https://doi.org/10.1016/j.cemconcomp.2010.10.021
[9] C. Duran Atiş, C. Bilim, Ö. Çelik, O. Karahan, Influence of activator on the strength and drying shrinkage of alkali-activated slag mortar, Constr. Build. Mater. (2009) 23: 548-555. https://doi.org/10.1016/j.conbuildmat.2007.10.011
[10] A. Fernández-Jiménez, F. Puertas, Effect of activator mix on the hydration and strength behaviour of alkali-activated slag cements, Adv. Cem. Res. (2003) 15: 129-136. https://doi.org/10.1680/adcr.2003.15.3.129
[11] B. Walkley, X. Ke, J.L. Provis, S.A. Bernal, Activator anion influences the nanostructure of alkali-activated slag cements, J. Phys. Chem. C. (2021) 125: 20727-20739. https://doi.org/10.1021/acs.jpcc.1c07328
[12] M. Ben Haha, B. Lothenbach, G. Le Saout, F. Winnefeld, Influence of slag chemistry on the hydration of alkali-activated blast-furnace slag - Part I: Effect of MgO, Cem. Concr. Res. (2011) 41: 955-963. https://doi.org/10.1016/j.cemconres.2011.05.002
[13] A. Schöler, F. Winnefeld, M. Ben Haha, B. Lothenbach, The effect of glass composition on the reactivity of synthetic glasses, J. Am. Ceram. Soc. (2017) 100: 2553-2567. https://doi.org/10.1111/jace.14759
[14] M. Ben Haha, B. Lothenbach, G. Le Saout, F. Winnefeld, Influence of slag chemistry on the hydration of alkali-activated blast-furnace slag - Part II: Effect of Al₂O₃, Cem. Concr. Res. (2012) 42: 74-83. https://doi.org/10.1016/j.cemconres.2011.08.005
[15] S. Kucharczyk, M. Sitarz, M. Zajac, J. Deja, The effect of CaO/SiO2 molar ratio of CaO-Al₂O₃-SiO₂ glasses on their structure and reactivity in alkali activated system, Spectrochim. Acta - Part A Mol. Biomol. Spectrosc. (2018) 194: 163-171. https://doi.org/10.1016/j.saa.2018.01.018
[16] B. Walkley, R. San Nicolas, M.A. Sani, S.A. Bernal, J.S.J. van Deventer, J.L. Provis, Structural evolution of synthetic alkali-activated CaO-MgO-Na₂O-Al₂O₃-SiO₂ materials is influenced by Mg content, Cem. Concr. Res. (2017) 99: 155-171. https://doi.org/10.1016/j.cemconres.2017.05.006
[17] M. Criado, B. Walkley, X. Ke, J.L. Provis, S.A. Bernal, Slag and activator chemistry control the reaction kinetics of sodium metasilicate-activated slag cements, Sustain. (2018) 10. https://doi.org/10.3390/su10124709
[18] Y. Chen, Z. Shui, W. Chen, Q. Li, G. Chen, Effect of MgO content of synthetic slag on the formation of Mg-Al LDHs and sulfate resistance of slag-fly ash-clinker binder, Constr. Build. Mater. (2016) 125: 766-774. https://doi.org/10.1016/j.conbuildmat.2016.08.086
[19] H. Xu, J.S.J. Van Deventer, The geopolymerisation of alumino-silicate minerals, Int. J. Miner. Process. (2000) 59: 247-266. https://doi.org/10.1016/S0301-7516(99)00074-5
[20] A. Hamdan, T. Kim, A. Hajimohammadi, Reaction kinetics in alkali-activated slag: The role of minor oxides, in: Concr. Inst. Aust. Bienn. Natl. Conf. 2021.
[21] J.L. Provis, S.A. Bernal, Geopolymers and Related Alkali-Activated Materials, Annu. Rev. Mater. Res. (2014) 44: 299-327. https://doi.org/10.1146/annurev-matsci-070813-113515
[22] K.L. Scrivener, A. Capmas, Lea's Chemistry of Cement and Concrete : Chapter 13, 2004.
[23] A. Hamdan, T. Kim, A. Hajimohammadi, F.M. Alnahhal, A. Rawal, Synthesis of chemically controlled cementitious materials using organic steric entrapment (OSE) method: Process, advantages, and characterisation, Cem. Concr. Res. (2022) 153. https://doi.org/10.1016/j.cemconres.2021.106698
[24] O.E. Gjorv, Alkali activation of a Norwegian granulated blast furnace slag, Am. Concr. Institute, ACI Spec. Publ. SP-114 (1989) 1501-1517. https://doi.org/10.14359/1862
[25] J. Bijen, H. Waltje, Alkali activated slag-fly ash cements, Am. Concr. Institute, ACI Spec. Publ. SP-114 (1989) 1565-1578. https://doi.org/10.14359/1900

[26] S. dong Wang, Review of recent research on alkali-activated concrete in China, Mag. Concr. Res. (1991) 43: 29-35.
https://doi.org/10.1680/macr.1991.43.154.29

[27] S.D. Wang, K.L. Scrivener, P.L. Pratt, Factors affecting the strength of alkali-activated slag, Cem. Concr. Res. (1994) 24: 1033-1043.
https://doi.org/10.1016/0008-8846(94)90026-4

[28] B. Yuan, Q.L. Yu, H.J.H. Brouwers, Evaluation of slag characteristics on the reaction kinetics and mechanical properties of Na_2CO_3 activated slag, Constr. Build. Mater. (2017) 131: 334-346.
https://doi.org/10.1016/j.conbuildmat.2016.11.074

[29] E.C. Arvaniti, M.C.G. Juenger, S.A. Bernal, J. Duchesne, L. Courard, S. Leroy, J.L. Provis, A. Klemm, N. De Belie, Determination of particle size, surface area, and shape of supplementary cementitious materials by different techniques, Mater. Struct. (2015) 48: 3687-3701. https://doi.org/10.1617/s11527-014-0431-3

[30] S. Brunauer, P.H. Emmett, E. Teller, Adsorption of Gases in Multimolecular Layers, J. Am. Chem. Soc. (1938) 60: 309-319.
https://doi.org/10.1021/ja01269a023

[31] N.J. Clayden, S. Esposito, A. Aronne, P. Pernice, Solid state 27Al NMR and FTIR study of lanthanum aluminosilicate glasses, J. Non. Cryst. Solids. (1999) 258: 11-19.
https://doi.org/10.1016/S0022-3093(99)00555-4

[32] S.-L. Lin, C.-S. Hwang, Structures of CeO_2-Al_2O_3-SiO_2 glasses, J. Non. Cryst. Solids. (1996) 202: 61-67.
https://doi.org/10.1016/0022-3093(96)00138-X

[33] R.L.D. C. Shi, A calorimetric study of early hydration of alkali-slag cements, Cem. Concr. Res. (1995) 25: 1333-1346.
https://doi.org/10.1016/0008-8846(95)00126-W

[34] Y. Zuo, G. Ye, Preliminary interpretation of the induction period in hydration of sodium hydroxide/silicate activated slag, Materials (Basel). (2020) 13: 1-19. https://doi.org/10.3390/ma13214796

[35] D. Ravikumar, N. Neithalath, Reaction kinetics in sodium silicate powder and liquid activated slag binders evaluated using isothermal calorimetry, Thermochim. Acta. (2012) 546: 32-43.
https://doi.org/10.1016/j.tca.2012.07.010

[36] A. Ehrenberg, N. Romero Sarcos, D. Hart, H. Bornhöft, J. Deubener, Influence of the Thermal History of Granulated Blast Furnace Slags on Their Latent Hydraulic Reactivity in Cementitious Systems, J. Sustain. Metall. (2020) 6: 207-215.
https://doi.org/10.1007/s40831-020-00269-4

[37] N. Pronina, S. Krüger, H. Bornhöft, J. Deubener, A. Ehrenberg, Cooling history of a wet-granulated blast furnace slag (GBS), J. Non. Cryst. Solids. (2018) 499: 344-349.
https://doi.org/10.1016/j.jnoncrysol.2018.07.054

[38] Arun K. Varshneya, J.C. Mauro, Fundamentals of Inorganic Glasses, 3rd Ed., Elsevier, 2019.
https://doi.org/10.1016/C2017-0-04281-7

[39] A. Fernández-Jiménez, J.G. Palomo, F. Puertas, Alkali-activated slag mortars: Mechanical strength behaviour, Cem. Concr. Res. (1999) 29: 1313-1321. https://doi.org/10.1016/S0008-8846(99)00154-4